Scalar Potentials and the Dirac Equation

Bastian Bergerhoff

Gesellschaft für Schwerionenforschung (GSI), Planckstraße 1, Postfach 110 552,
D-64220 Darmstadt, Federal Republic of Germany

Gerhard Soff

Institut für Theoretische Physik, Technische Universität, 01062 Dresden,
Federal Republic of Germany

Z. Naturforsch. **49 a,** 997–1012(1994); received October 5, 1994

The Dirac equation is solved for various types of scalar potentials. Energy eigenvalues and normalized bound-state wave functions are calculated analytically for a scalar $1/r$-potential as well as for a mixed scalar and Coulomb $1/r$-potential. Also continuum wave functions for positive and negative energies are derived. Similarly, we investigate the solutions of the Dirac equation for a scalar square-well potential. Relativistic wave functions for scalar Yukawa and exponential potentials are determined numerically. Finally, we also discuss solutions of the Dirac equation for scalar linear and quadratic potentials which are frequently used to simulate quark confinement.

1. Introduction

Scalar potentials are coupled to the mass of a spin-$\frac{1}{2}$-particle in the Dirac equation and thus act effectively as a position dependent mass. In contrast to this the minimal coupling of the electromagnetic potentials is correlated with the momentum. In this paper we explore in more detail the strong coupling limit and determine maximum binding energies in scalar potentials. The absence of the Klein paradox and of spontaneous pair creation [1] is emphasized. This represents one of the most intruiging pecularities of scalar interactions in distinction, e.g., to the minimal coupling of electromagnetic potentials.

In principle even long-range scalar interactions can not be ruled out in nature. However, maximum values for the coupling constants can be deduced from precision measurements in atomic spectroscopy and in quantum electrodynamics that put very stringent limits on the variety of possible scalar interactions. The exchange of a new scalar particle [2], [3] has been proposed to account for various unexplained phenomena in atomic physics. Again, from precision spectroscopy there is no evidence for any scalar interaction. On the other hand, scalar potentials that increase with the radial distance are frequently employed in naive quark models due to their confinement properties. It is worthwhile to note that analytical solutions of the Dirac equation for a scalar harmonic oscillator potential can be derived, in contrast to a minimal coupling as the zeroth component of a four-vector.

Unlike its nonrelativistic counterpart, the Dirac equation can be solved analytically only for a rather restricted class of potentials. Among them is the $1/r$-Coulomb potential which determines the gross features of the hydrogen spectrum. One further motivation for our considerations is to derive additional solutions of this fundamental equation of motion which, e.g., governs the theory of atomic structure. Calculated energy eigenvalues and wave functions are compared with published results [1], [4]-[13]. Furthermore we refer to solutions of the Dirac equation for scalar potentials as published in [14]-[18].

Our paper is organized as follows: In the next section we introduce the fundamental differential equations and define our notation. In Sect. 3 solutions of the Dirac equation for scalar $1/r$-potentials are discussed. As a new feature we evaluate normalized bound state wave functions and derive continuum state wave functions which are normalized on the energy scale. Special emphasis is laid on strong coupling constants $Z\alpha$ with the Sommerfeld fine structure constant $\alpha \approx 1/137$. Section 4 deals with solutions of this relativistic wave equation for a superposition of a scalar and a Coulomb-like coupled $1/r$-potential.

Reprint requests to Prof. Dr. G. Soff.

0932-0784 / 94 / 1100-0997 $ 06.00 © – Verlag der Zeitschrift für Naturforschung, D-72072 Tübingen

A few misprints in the current literature are corrected. As a particular example for a short range scalar potential that can be treated analytically we study the one- as well as the three-dimensional square-well potential in Section 5. Again we predominantly concentrate on bound-state solutions for strong scalar couplings. The subsequent section briefly reviews analytical solutions for linear and quadratic potentials that as a most exciting feature exhibit confinement properties being utilized in naive quark models. To describe the exchange of a possible scalar particle with mass μ we also explore numerical solutions of the Dirac equation for scalar Yukawa and exponential potentials. Finally we present a brief summary.

2. Premises

We will treat several spherically symmetric scalar potentials $V(r)$. Using units with $\hbar = c = 1$, the stationary Dirac equation reads [1]

$$\left[\hat{\vec{\alpha}}\hat{\vec{p}} + \hat{\beta}\,(m_0 + V(r))\right]\psi = E\psi, \tag{1}$$

where the standart representation of the Dirac matrices is employed [1], [19], i.e.

$$\hat{\vec{\alpha}} = \begin{pmatrix} 0 & \vec{\sigma} \\ \vec{\sigma} & 0 \end{pmatrix}, \quad \hat{\beta} = \begin{pmatrix} 1 & 0 \\ 0 & -1 \end{pmatrix}. \tag{2}$$

It is well known that (1) can be seperated for spherically symmetric potentials. Using the spherical spinors [19]

$$\chi_{\kappa,\mu} = \sum_{m=\pm\frac{1}{2}} (l\ 1/2\ j \mid \mu - m, m) \times Y_{l,\mu-m}(\theta,\phi)\,\chi_m, \tag{3}$$

where $\chi_{\frac{1}{2}} = \begin{pmatrix} 1 \\ 0 \end{pmatrix}$ and $\chi_{-\frac{1}{2}} = \begin{pmatrix} 0 \\ 1 \end{pmatrix}$, we start from the separation ansatz

$$\psi(\vec{r}) = \begin{pmatrix} g(r)\,\chi_{\kappa,\mu}(\theta,\phi) \\ i f(r)\,\chi_{-\kappa,\mu}(\theta,\phi) \end{pmatrix}. \tag{4}$$

In Sect. 4 we will also discuss the bound state solutions of the Dirac equation with a superposition of a scalar and a Coulomb-like coupled $1/r$-potential. The radial equations then read

$$\frac{\mathrm{d}}{\mathrm{d}r}G = -\frac{\kappa}{r}G + [E + m_0 + V_\mathrm{s}(r) - V_\mathrm{c}(r)]\,F,$$

$$\frac{\mathrm{d}}{\mathrm{d}r}F = \frac{\kappa}{r}F - [E - m_0 - V_\mathrm{s}(r) - V_\mathrm{c}(r)]\,G, \tag{5}$$

where $V_\mathrm{s}(r)$ and $V_\mathrm{c}(r)$ denote the scalar and Coulomb-like coupled potentials, respectively. Here and in the following we abbreviate $G(r) = rg(r)$ and $F(r) = rf(r)$. κ denotes the eigenvalue of the operator [19] $\hat{\kappa} = \hat{\beta}\left(\hat{\vec{\sigma}}\hat{\vec{L}} + 1\right)$. It results $\left(\hat{\vec{\sigma}}\hat{\vec{L}} + 1\right)\chi_{\pm\kappa,\mu} = \mp\kappa\,\chi_{\pm\kappa,\mu}$. Furthermore, one finds the following dependence of κ on j and l, the total and the orbital angular momentum, respectively:

$$\kappa = \begin{cases} l & \text{for } j = l - \frac{1}{2}, \\ -l - 1 & \text{for } j = l + \frac{1}{2}. \end{cases} \tag{6}$$

We also indicate a second order differential equation for $g(r)$. One obtains

$$\begin{aligned} 0 &= \frac{\mathrm{d}^2}{\mathrm{d}r^2}g + \frac{2}{r}\frac{\mathrm{d}}{\mathrm{d}r}g - \frac{\kappa(\kappa+1)}{r^2}g \\ &\quad - \frac{1}{E + m_0 + V(r)}\left(\frac{\mathrm{d}}{\mathrm{d}r}V(r)\right) \\ &\quad \times \left(\frac{\mathrm{d}}{\mathrm{d}r}g + \frac{\kappa+1}{r}g\right) \\ &\quad + \left\{E^2 - (m_0 + V(r))^2\right\}g, \\ f &= \frac{1}{E + m_0 + V(r)}\frac{1}{r}\left(r\frac{\mathrm{d}}{\mathrm{d}r}g + (\kappa+1)g\right). \end{aligned} \tag{7}$$

It will also be useful to define

$$l_\kappa = \begin{cases} \kappa & \text{for } \kappa > 0, \\ -\kappa - 1 & \text{for } \kappa < 0. \end{cases} \tag{8}$$

The bound state wave functions will be normalized according to

$$\int_0^\infty \mathrm{d}r\, r^2\,(f^2 + g^2) = 1, \tag{9}$$

while the continuum wave functions are normalized on the energy scale, i.e. according to

$$\begin{aligned} \int \psi^\dagger_{E'}\psi_E\,\mathrm{d}^3r &= \int_0^\infty \mathrm{d}r\, r^2\,(f_E\,f_{E'} + g_E\,g_{E'}) \\ &= \delta(E' - E). \end{aligned} \tag{10}$$

3. $1/r$-potential

As a particular example for a long-range potential we investigate the solutions of the Dirac equation for a scalar $1/r$-potential,

$$V(r) = -\frac{Z\alpha}{r}. \tag{11}$$

Here α denotes the fine structure constant, $Z\alpha$ is chosen as coupling constant for convenience, since it simplifies the comparison with the Coulomb case.

The bound state energies and unnormalized wave functions are given by Vasconcelos [4] as well as in [1], [11], [12]. We will derive them here for the sake of completeness. Let $\lambda = \left(m_0^2 - E^2\right)^{1/2}$ and $\varrho = 2\lambda r$.

The wave functions and energies are obtained utilizing the ansatz

$$\begin{aligned} G(\varrho) &= (m_0 + E)^{1/2} e^{-\varrho/2} \left(\phi_1(\varrho) + \phi_2(\varrho)\right), \\ F(\varrho) &= (m_0 - E)^{1/2} e^{-\varrho/2} \left(\phi_1(\varrho) - \phi_2(\varrho)\right). \end{aligned} \tag{12}$$

By examining the radial differential equation close to the origin, one finds for $r \to 0$ the solutions $G(\varrho) = a\varrho^\gamma$ and $F(\varrho) = b\varrho^\gamma$ where

$$\gamma = +\sqrt{\kappa^2 + (Z\alpha)^2}. \tag{13}$$

The negative square root has to be ruled out since in order for the wave functions to be normalizable the integral (9) has to be finite. To this end, $\gamma > -1$ has to hold. But since $\kappa^2 \geq 1$ and, in contrast to the Coulomb case, $(Z\alpha)^2$ is added , only the positive square root leads to normalizable wave functions. With (12) one derives that if

$$\begin{aligned} \phi_1(\varrho) &= \varrho^\gamma \sum_{m=0}^{\infty} A_m \varrho^m, \\ \phi_2(\varrho) &= \varrho^\gamma \sum_{m=0}^{\infty} B_m \varrho^m, \end{aligned} \tag{14}$$

the following relations for the coefficients A_m and B_m must hold:

$$\frac{B_0}{A_0} = \frac{\kappa - Z\alpha E/\lambda}{n'}, \tag{15}$$

as well as

$$A_m = \frac{(1-n')(2-n')\ldots(m-n')}{m!(2\gamma+1)\ldots(2\gamma+m)} A_0,$$

$$B_m = (-1)^m \frac{n'(n'-1)\ldots(n'-m+1)}{m!(2\gamma+1)\ldots(2\gamma+m)} B_0 \tag{16}$$

with $n' = Z\alpha m_0/\lambda - \gamma$. These are the defining relations of the confluent hypergeometric functions, therefore one arrives at

$$\begin{aligned} \phi_1(\varrho) &= A_0 \varrho^\gamma {}_1F_1\left(1-n', 2\gamma+1; \varrho\right), \\ \phi_2(\varrho) &= \frac{\kappa - Z\alpha E/\lambda}{n'} A_0 \varrho^\gamma \\ &\quad \times {}_1F_1\left(-n', 2\gamma+1; \varrho\right). \end{aligned} \tag{17}$$

In order to obtain a normalizable solution (12), n' has to be a positive integer, or zero. This requirement leads to the energy eigenvalues

$$E = \pm m_0 \sqrt{1 - \frac{(Z\alpha)^2}{(n - j - 1/2 + \gamma)^2}}, \tag{18}$$

where $n = n' + j + 1/2$ is the principal quantum number of the state. Observe that (13), (15) and (17) differ from those obtained for the Coulomb potential only by the sign of $(Z\alpha)^2$ in (13) and by the interchange of E with m_0. Bearing this in mind, it is straightforward to derive the normalized bound-state wave functions, following the procedure as in the Coulomb case (see e.g. [20]). Thus the positive energy solutions read

$$g(r) = k_+(A - B) \tag{19}$$

and

$$f(r) = -k_-(A + B), \tag{20}$$

where

$$\begin{aligned} k_\pm &= \frac{(2\lambda)^{3/2}}{\Gamma(2\gamma+1)} (2\lambda r)^{\gamma-1} e^{-\lambda r} \\ &\quad \times \sqrt{\frac{(m_0 \pm E)\,\Gamma(2\gamma+n'+1)}{4m_0\,(EZ\alpha/\lambda)\,(EZ\alpha/\lambda - \kappa)\,n'!}}, \\ A &= (EZ\alpha/\lambda - \kappa)\,{}_1F_1(-n', 2\gamma+1; 2\lambda r), \\ B &= n'\,{}_1F_1(1-n', 2\gamma+1; 2\lambda r). \end{aligned}$$

A numerical evaluation of the radial wave functions (19) and (20) verifies the normalization condition (9) within the numerical accuracy.

The negative energy solutions are obtained by observing that the radial differential equations are symmetric under the interchange of f with g and

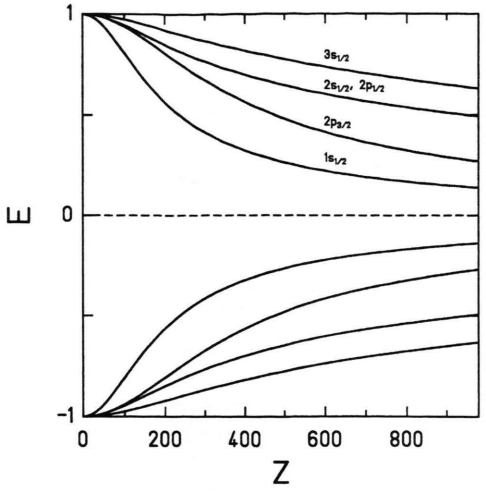

Fig. 1. Bound state energies in a long-range scalar potential of the form $V(r) = -Z\alpha/r$. Natural units are used ($\hbar = c = m_0 = 1$).

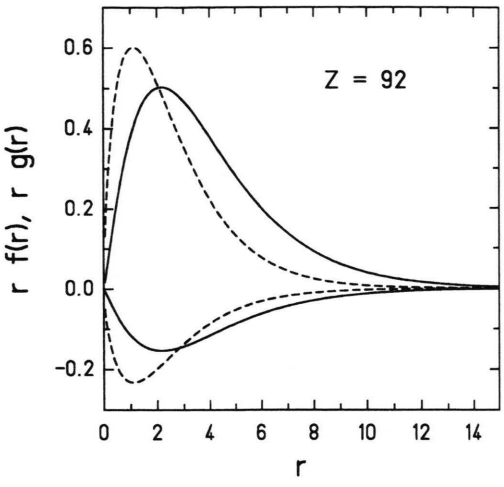

Fig. 2. The large component $G(r) = rg(r)$ (positive values) and the small component $F(r) = rf(r)$ (negative values) of a 1s-wave function in a Coulomb potential (dashed lines) and in a scalar $1/r$-potential (solid lines) are depicted. Natural units are used.

the simultanous replacement of E by $-E$ and κ by $-\kappa$ (see e.g. [19]). We thus find $g(-E,-\kappa,r) = f(E,\kappa,r)$ and $f(-E,-\kappa,r) = g(E,\kappa,r)$.

The energy spectrum is displayed in Figure 1. It can be concluded that the vacuum remains stable for a pure scalar coupling, no pair creation occurs, whatever the coupling strength is. It is also worth mentioning that the ordering of the levels differs from that for Coulomb-like potentials: The $2p_{3/2}$-state is bound more strongly than the $2p_{1/2}$-state. Figures 2 and 3 demonstrate the formal resemblance of the positive energy wave functions in scalar and Coulomb-like coupled $1/r$-potentials. The solid lines display the large and small components in the scalar potential treated above, the dashed lines represent the radial wave functions in a Coulomb potential of equal strength. Figure 2 corresponds to an 1s-state, while Fig. 3 depicts the radial wave functions for a $2p_{3/2}$-state. There is of course a fundamental difference between the two types of couplings: while a Coulomb potential has either particle or antiparticle bound states, the scalar potential can always have both.

We now discuss the calculation of continuum states. To begin with, we define

$$\begin{aligned} p &= \left(E^2 - m_0^2\right)^{1/2} \equiv i\lambda, \\ x &= 2ipr. \end{aligned} \tag{21}$$

Observe that p is real, so that x is purely imaginary. We will compute states that describe spherical standing waves as $r \to \infty$, so κ remains a good quantum number. First we restrict ourselves to positive energy states, that is $E > m_0$. The solutions for $E < -m_0$ will be obvious from the derived results. We make the ansatz

$$\begin{aligned} G(x) &= (E+m_0)^{1/2}\left(\varphi_1(x) + \varphi_2(x)\right), \\ F(x) &= i\,(E-m_0)^{1/2}\left(\varphi_1(x) - \varphi_2(x)\right). \end{aligned} \tag{22}$$

One obtains two equations for the φ_i's:

$$\begin{aligned} \frac{\mathrm{d}}{\mathrm{d}x}\varphi_1 &= \left(\frac{1}{2} + \frac{im_0Z\alpha}{px}\right)\varphi_1 - \left(\frac{\kappa}{x} - \frac{iEZ\alpha}{px}\right)\varphi_2, \\ \frac{\mathrm{d}}{\mathrm{d}x}\varphi_2 &= -\left(\frac{\kappa}{x} + \frac{iEZ\alpha}{px}\right)\varphi_1 \\ &\quad - \left(\frac{1}{2} + \frac{im_0Z\alpha}{px}\right)\varphi_2. \end{aligned} \tag{23}$$

Since we want to derive standing waves at infinity, comparison of (23) and their complex conjugate leads to the requirement $\varphi_1^* = \varphi_2$. We thus have to solve (23) for φ_1, leaving a phase that can be chosen such that φ_2 satisfies (23). Combining (23) we get

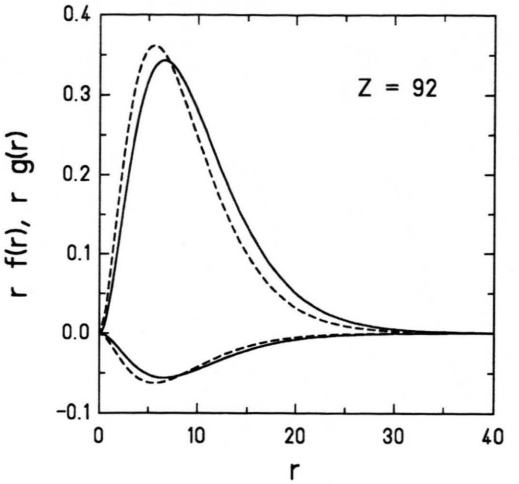

Fig. 3. Same as Fig. 2, but for a $2p_{3/2}$ -state.

$$\frac{\mathrm{d}^2}{\mathrm{d}x^2}\varphi_1 + \frac{1}{x}\frac{\mathrm{d}}{\mathrm{d}x}\varphi_1 - \left\{\tfrac{1}{4} + \left(\tfrac{1}{2} + \tfrac{im_0 Z\alpha}{p}\right)\tfrac{1}{x} + \tfrac{\gamma^2}{x^2}\right\}\varphi_1 = 0, \quad (24)$$

where γ is as defined in (13). Substituting $\varphi_1(x) = x^{-1/2}M(x)$ provides the following equation for M:

$$\frac{\mathrm{d}^2}{\mathrm{d}x^2}M(x) - \left\{\frac{1}{4} + \left(\frac{1}{2} + \frac{im_0 Z\alpha}{p}\right)\frac{1}{x} + \frac{\gamma^2 - 1/4}{x^2}\right\}M(x) = 0. \quad (25)$$

The solution of (25) which is regular at the origin ($x = 0$) is the Whittaker function [21]

$$M_{-(iy+1/2),\gamma}(x) = x^{\gamma+1/2}\, e^{-x/2} \times {}_1F_1(\gamma + 1 + iy, 2\gamma + 1; x), \quad (26)$$

where $y = m_0 Z\alpha/p$. Resubstitution leads to

$$\varphi_1(r) = N(\gamma + iy)\, e^{i\eta}(2pr)^\gamma\, e^{-ipr} \times {}_1F_1(\gamma + 1 + iy, 2\gamma + 1; 2ipr), \quad (27)$$

where $N(\gamma + iy)$ is chosen for convenience, N is determined by normalization and $e^{i\eta}$ is the phase factor mentioned above.

We will now determine the phase factor from (23). Let

$$\varphi(r) = r^\gamma\, e^{-ipr} \times {}_1F_1(\gamma + 1 + iy, 2\gamma + 1; 2ipr). \quad (28)$$

It follows

$$e^{2i\eta} = \frac{iy\,(E/m_0) - \kappa}{\gamma + iy}. \quad (29)$$

In summary it results

$$G(r) = (E + m_0)^{1/2}\, N(2pr)^\gamma \{(\gamma + iy)e^{-ipr+i\eta} \times {}_1F_1(1 + \gamma + iy, 2\gamma + 1; 2ipr) + c.c.\} \quad (30)$$

and

$$F(r) = i\,(E - m_0)^{1/2}\, N(2pr)^\gamma \{(\gamma + iy)e^{-ipr+i\eta} \times {}_1F_1(1 + \gamma + iy, 2\gamma + 1; 2ipr) - c.c.\}, \quad (31)$$

where $c.c.$ stands for the complex conjugate.

We now turn to the normalization of the continuum wave functions. We want to normalize (30) and (31) 'on the energy scale', i.e. according to (10). This is to be understood asymptotically, since it turns out that the scattering phase is r-dependent in basically the same way as in the Coulomb case. For $r \to \infty$ we want F and G to assume the form

$$\begin{aligned} G &= A\,(E + m_0)^{1/2}\cos(pr + \delta), \\ F &= A\,(E - m_0)^{1/2}\sin(pr + \delta). \end{aligned} \quad (32)$$

From (22) it follows for $r \to \infty$, $\varphi_1(r) = \frac{1}{2}A \exp(i(pr + \delta))$. By using the asymptotic behaviour of the confluent hypergeometric function (32) are satisfied if

$$\delta = y \ln(2pr) - \arg(\Gamma(\gamma + iy)) - \frac{\pi\gamma}{2} + \eta \quad (33)$$

and

$$A = \frac{2Ne^{-\pi y/2}\,\Gamma(2\gamma + 1)}{|\,\Gamma(\gamma + iy)\,|}. \quad (34)$$

δ can be chosen to satisfy (33), N will now be computed, via A, from (10), (32), and (34). Exactly as in the case for the Coulomb potential [19] it follows

$$A = \frac{1}{\sqrt{\pi p}}, \quad (35)$$

which finally yields

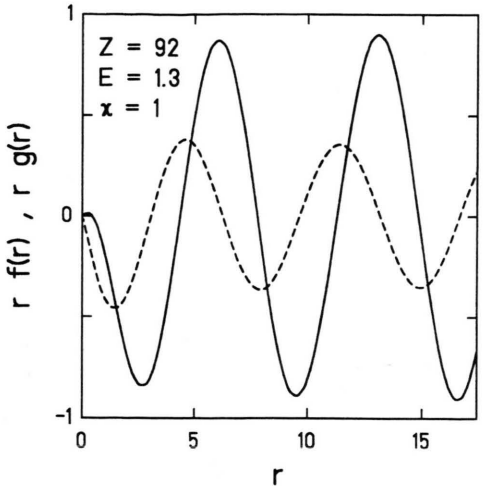

Fig. 4. Continuum wave function ($E = 1.3, \kappa = 1$) in a scalar $1/r$-potential with the coupling constant $Z = 92$. Natural units are used. The solid line depicts $rg(r)$ while the dashed line indicates $rf(r)$.

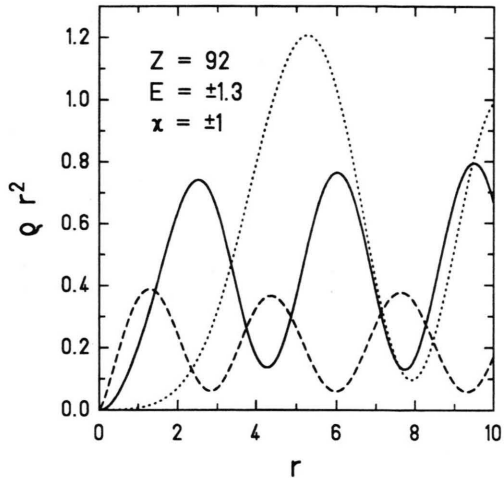

Fig. 5. Probability densities $\varrho r^2 = F^2(r) + G^2(r)$ of a particle with $E = \pm 1.3, \kappa = \pm 1$ in a scalar $1/r$-potential (solid line) compared to the densities in a Coulomb potential (the dashed line represents the positive, the dotted line the negative energy state).

$$N = \frac{e^{\pi y/2} \mid \Gamma(\gamma + iy) \mid}{2\sqrt{\pi p}\,\Gamma(2\gamma + 1)}. \tag{36}$$

The radial wave functions for positive energies read

$$G(r) = \sqrt{E + m_0}\frac{e^{\pi y/2} \mid \Gamma(\gamma + iy) \mid (2pr)^\gamma}{2\sqrt{\pi p}\,\Gamma(2\gamma + 1)} \times \{(\gamma + iy)e^{-ipr+i\eta} \times {}_1F_1(1 + \gamma + iy, 2\gamma + 1; 2ipr) + c.c.\} \tag{37}$$

and

$$F(r) = i\sqrt{E - m_0}\frac{e^{\pi y/2} \mid \Gamma(\gamma + iy) \mid (2pr)^\gamma}{2\sqrt{\pi p}\,\Gamma(2\gamma + 1)} \times \{(\gamma + iy)e^{-ipr+i\eta} \times {}_1F_1(1 + \gamma + iy, 2\gamma + 1; 2ipr) - c.c.\}. \tag{38}$$

To obtain the negative energy solutions, observe that under the replacement of E by $-E$ and κ by $-\kappa$ the quantities γ and y remain unchanged, while from (29) $e^{2i\eta} \to -e^{2i\eta}$, and thus $e^{i\eta} \to i\,e^{i\eta}$. Interchanging F with G, the negative energy solutions then read

$$G(r) = \sqrt{-E - m_0}\frac{e^{\pi y/2} \mid \Gamma(\gamma + iy) \mid (2pr)^\gamma}{2\sqrt{\pi p}\,\Gamma(2\gamma + 1)} \times \{(\gamma + iy)e^{-ipr+i\eta} \times {}_1F_1(1 + \gamma + iy, 2\gamma + 1; 2ipr) + c.c.\} \tag{39}$$

and

$$F(r) = -i\sqrt{-E + m_0}\frac{e^{\pi y/2} \mid \Gamma(\gamma + iy) \mid (2pr)^\gamma}{2\sqrt{\pi p}\,\Gamma(2\gamma + 1)} \times \{(\gamma + iy)e^{-ipr+i\eta} \times {}_1F_1(1 + \gamma + iy, 2\gamma + 1; 2ipr) - c.c.\}, \tag{40}$$

where the overall phase is determined by the normalization condition (10).

A few examples for radial continuum wave functions are depicted in Figs. 4 and 5. In Fig. 4 a positive energy state with $E = 1.3\,m_0$ and $\kappa = 1$ is displayed. The coupling strength is chosen to be 92α. Observe the interchange of F with G corresponding to the sign changes of E and κ for the negative energy solutions.

The probability densities $F^2(r) + G^2(r)$ of Coulomb wave functions are compared to those evaluated here in Figure 5. Here the solid line corresponds to a scalar potential, the dashed line displays the density

of an electron, while the dotted line shows the density of the negative energy state, both in a Coulomb potential. Again, for the scalar potential we have the same density for particle and anti-particle states, while the Coulomb potential distinguishes these cases.

4. Superposition of a scalar and a Coulomb-like coupled $1/r$-potential

We examine the bound state solutions of the Dirac equation with a scalar potential

$$V_s(r) = -\frac{Z'\alpha}{r} \tag{41}$$

and a Coulomb potential of a point nucleus

$$V_c(r) = -\frac{Z\alpha}{r}, \tag{42}$$

coupled as the time-like component of a four-vector. The corresponding radial equations are given by (5). By the same reasoning as in Sect. 3 one employs the ansatz (12). With (5) the resulting equations for the ϕ_i's are

$$\begin{aligned}\frac{\mathrm{d}}{\mathrm{d}\varrho}\phi_1 &= \left(1 - \frac{Z'\alpha m_0}{\lambda\varrho} - \frac{Z\alpha E}{\lambda\varrho}\right)\phi_1 \\ &\quad - \left(\frac{\kappa}{\varrho} + \frac{Z\alpha m_0}{\lambda\varrho} + \frac{Z'\alpha E}{\lambda\varrho}\right)\phi_2, \\ \frac{\mathrm{d}}{\mathrm{d}\varrho}\phi_2 &= \left(\frac{Z\alpha m_0}{\lambda\varrho} + \frac{Z'\alpha E}{\lambda\varrho} - \frac{\kappa}{\varrho}\right)\phi_1 \\ &\quad + \left(\frac{Z'\alpha m_0}{\lambda\varrho} + \frac{Z\alpha E}{\lambda\varrho}\right)\phi_2. \end{aligned} \tag{43}$$

For $r \to 0$, we find

$$\gamma = +\sqrt{\kappa^2 + (Z'\alpha)^2 - (Z\alpha)^2}. \tag{44}$$

In this case, formally normalizable solutions exist for negative γ, provided $|\ \kappa\ | = 1$ and

$$Z^2 - Z'^2 \geq \frac{3}{4\alpha^2}. \tag{45}$$

Equation (44) leads, again in analogy to Sect. 3, to the ansatz (14) for the ϕ_i's. From this ansatz and (43) one obtains the following relations for the coefficients A_0 and B_0:

$$\frac{B_0}{A_0} = \frac{\kappa - Z\alpha m_0/\lambda - Z'\alpha E/\lambda}{n'} \tag{46}$$

and A_m and B_m as provided in (16). But here we have

$$n' = \frac{Z\alpha E}{\lambda} + \frac{Z'\alpha m_0}{\lambda} - \gamma. \tag{47}$$

Thus the same reasoning as in Sect. 3 leads to the energy eigenvalues

$$\begin{aligned} E = m_0 \Bigg\{ &-\frac{(Z\alpha)(Z'\alpha)}{(Z\alpha)^2 + (n - j - 1/2 + \gamma)^2} \\ &\pm \Bigg[\left(\frac{(Z\alpha)(Z'\alpha)}{(Z\alpha)^2 + (n - j - 1/2 + \gamma)^2} \right)^2 \\ &- \frac{(Z'\alpha)^2 - (n - j - 1/2 + \gamma)^2}{(Z\alpha)^2 + (n - j - 1/2 + \gamma)^2} \Bigg]^{1/2} \Bigg\}. \end{aligned} \tag{48}$$

Observing that the normalized wave functions should be the solutions of the Coulomb case if $Z' = 0$ and should reduce to eqs. (19), (20) if $Z = 0$, one derives the normalized solutions

$$g(r) = k_+(A - B) \tag{49}$$

and

$$f(r) = -k_-(A + B), \tag{50}$$

where

$$\begin{aligned} k_\pm &= \frac{(2\lambda)^{3/2}}{\Gamma(2\gamma + 1)} (2\lambda r)^{\gamma - 1} e^{-\lambda r} \\ &\quad \times \sqrt{\frac{(m_0 \pm E)\,\Gamma(2\gamma + n' + 1)}{4m_0 C(C - \kappa) n'!}}, \\ A &= (C - \kappa)\, {}_1F_1(-n', 2\gamma + 1; 2\lambda r), \\ B &= n'\, {}_1F_1(1 - n', 2\gamma + 1; 2\lambda r), \\ C &= (Z\alpha m_0 + Z'\alpha E)/\lambda. \end{aligned}$$

The energy spectrum of a superposition of a scalar $1/r$-potential and a Coulomb potential with equal

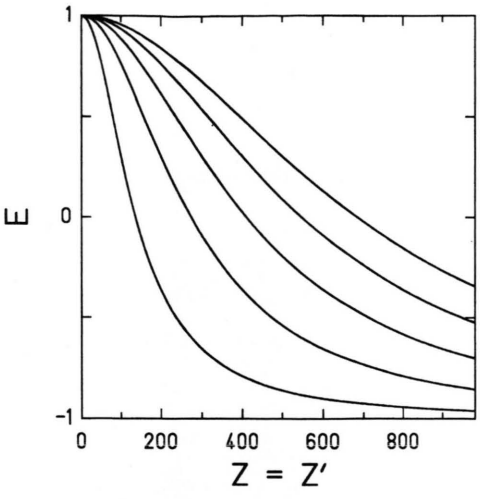

Fig. 6. Bound state energies in a superposition of scalar and Coulomb-like coupled $1/r$-potentials of equal strength. The strongest bound state is the 1s-state, the other curves represent states with increasing principal quantum number as the binding energy decreases.

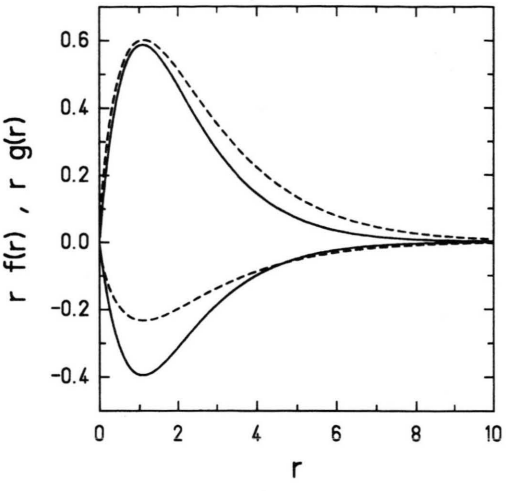

Fig. 7. The large and small components (positive and negative values, respectively) of a 1s-state in a superposition of scalar and Coulomb-like coupled potentials of equal strength ($Z = Z' = 92$) (solid lines) compared to the wave functions of the same state in a pure Coulomb potential of equal strength (dashed lines) are displayed.

strength is displayed in Figure 6. In this case, the negative sign of the square root in (48) has to be ruled out, since it leads to a solution $E = -m_0$, which is not compatible with (47). The eigenvalues approach $E = -m_0$ asymptotically, but in the absence of quantum fluctuations the vacuum again remains stable.

A bound state wave function corresponding to an 1s-state in a superposition of scalar and Coulomb-like coupled potentials with $Z = Z' = 92$ is depicted in Fig. 7 together with the wave function of the same state in a pure Coulomb potential of the same strength. Here the solid lines represent the large and small component of the radial wave function in the superposition potential, while the dashed lines display the Coulomb wave functions.

Considering continuum states, we can again closely follow Section 3. Starting from the radial equations (5) using the substitutions (21), one arrives at

$$\begin{aligned}\frac{\mathrm{d}}{\mathrm{d}x}G &= -\frac{\kappa}{x}G + \left[\frac{E+m_0}{2ip} + \frac{(Z-Z')\alpha}{x}\right]F,\\ \frac{\mathrm{d}}{\mathrm{d}x}F &= \frac{\kappa}{x}F - \left[\frac{E-m_0}{2ip} + \frac{(Z+Z')\alpha}{x}\right]G. \end{aligned} \quad (51)$$

The ansatz (22) yields the following differential equations for the φ_i's:

$$\begin{aligned}\frac{\mathrm{d}}{\mathrm{d}x}\varphi_1 &= \left(\frac{1}{2} + \frac{iEZ\alpha}{px} + \frac{im_0Z'\alpha}{px}\right)\varphi_1\\ &\quad - \left(\frac{\kappa}{x} - \frac{im_0Z\alpha}{px} - \frac{iEZ'\alpha}{px}\right)\varphi_2,\\ \frac{\mathrm{d}}{\mathrm{d}x}\varphi_2 &= -\left(\frac{\kappa}{x} + \frac{im_0Z\alpha}{px} + \frac{iEZ'\alpha}{px}\right)\varphi_1\\ &\quad - \left(\frac{1}{2} + \frac{iEZ\alpha}{px} + \frac{im_0Z'\alpha}{px}\right)\varphi_2. \end{aligned} \quad (52)$$

We again require $\varphi_2^* = \varphi_1$, thus calculating standing waves. Following Sect. 3, we derive a second order differential equation for φ_1,

$$\begin{aligned}&\frac{\mathrm{d}^2}{\mathrm{d}x^2}\varphi_1 + \frac{1}{x}\frac{\mathrm{d}}{\mathrm{d}x}\varphi_1 - \left\{\frac{1}{4}\right.\\ &\left. + \left(\frac{1}{2} + \frac{iEZ\alpha + im_0Z'\alpha}{p}\right)\frac{1}{x} + \frac{\gamma^2}{x^2}\right\}\varphi_1 = 0, \end{aligned} \quad (53)$$

which, after substituting $\varphi_1(x) = x^{-1/2}M(x)$, yields

$$\frac{\mathrm{d}^2}{\mathrm{d}x^2}M(x) - \left\{\frac{1}{4} + \left(\frac{1}{2} + \frac{im_0Z'\alpha + iEZ\alpha}{p}\right)\frac{1}{x} + \frac{\gamma^2 - 1/4}{x^2}\right\} M(x) = 0. \quad (54)$$

Identifying the solution of (54) to be the Whittaker function $M_{-(iy+1/2),\gamma}(x)$ (26), where $y = (m_0Z'\alpha + EZ\alpha)/p$, and proceeding as in Sect. 3, we finally arrive at the positive energy continuum wave functions (37), (38), where in this case γ is as in (44), and

$$e^{2i\eta} = \frac{1}{\gamma + iy}\left(\frac{i\alpha}{p}(m_0Z + EZ') - \kappa\right). \quad (55)$$

The negative energy continuum wave functions are, by the same reasoning as in Sect. 3, given by (39) and (40) with the appropriate changes in y, γ, and $e^{2i\eta}$ as indicated above. Please note again the interchange of F with G corresponding to the sign changes of E, κ and Z, since the charge of the particle is inverted by charge conjugation [19]. $e^{2i\eta}$ can be taken from (55) with the replacement $Z \to -Z$.

5. Square-well potential

We study the solution of the Dirac equation for a scalar square-well potential. We will demonstrate below that the energy eigenvalues exhibit a remarkable behavior for this potential both in one and three dimensions. We will first sketch the one-dimensional solution, which is found e.g. in [1].

Let

$$V(x) = \begin{cases} -V_0 & \text{for } -a/2 \le x \le a/2, \\ 0 & \text{else.} \end{cases} \quad (56)$$

We define three domains I ($x < -a/2$), II($-a/2 \le x \le a/2$) and III ($x > a/2$). In domains I and III, the momentum is given by

$$k_1^2 = E^2 - m_0^2, \quad (57)$$

while in domain II we have

$$k_2^2 = E^2 - (m_0 - V_0)^2. \quad (58)$$

The wave functions read

$$\psi_I = A\,e^{ik_1x}\begin{pmatrix} 1 \\ 0 \\ \frac{k_1}{E+m_0} \\ 0 \end{pmatrix} + A'\,e^{-ik_1x}\begin{pmatrix} 1 \\ 0 \\ -\frac{k_1}{E+m_0} \\ 0 \end{pmatrix}, \quad x < -a/2,$$

$$\psi_{II} = B\,e^{ik_2x}\begin{pmatrix} 1 \\ 0 \\ \frac{k_2}{E+m_0-V_0} \\ 0 \end{pmatrix} + B'\,e^{-ik_2x}\begin{pmatrix} 1 \\ 0 \\ -\frac{k_2}{E+m_0-V_0} \\ 0 \end{pmatrix}, \quad -a/2 \le x \le a/2, \quad (59)$$

and

$$\psi_{III} = C\,e^{ik_1x}\begin{pmatrix} 1 \\ 0 \\ \frac{k_1}{E+m_0} \\ 0 \end{pmatrix} + C'\,e^{-ik_1x}\begin{pmatrix} 1 \\ 0 \\ -\frac{k_1}{E+m_0} \\ 0 \end{pmatrix}, \quad x > a/2. \quad (60)$$

We have restricted ourselves to solutions with spin up only, because since the potential is spin-independent, no spin flip occurs and the spin-down solutions are thus obtained equivalently. Since the wave functions have to be continous at $x = \pm a/2$, it results

$$\begin{pmatrix} A \\ A' \end{pmatrix} = \frac{1}{4\gamma}\begin{pmatrix} r & s \\ \bar{s} & \bar{r} \end{pmatrix}\begin{pmatrix} C \\ C' \end{pmatrix}, \quad (61)$$

where

$$r = (1+\gamma)^2 e^{i(k_1-k_2)a} - (1-\gamma)^2 e^{i(k_1+k_2)a},$$

$$s = (1-\gamma^2)\left(e^{-ik_2a} - e^{ik_2a}\right),$$
$$\gamma = \frac{k_1}{E+m_0}\,\frac{E+m_0-V_0}{k_2}, \tag{62}$$

and $\bar{r}, \bar{s}$ are the complex conjugates of r and s. Considering bound states, we have $E^2 < m_0^2$, and k_1 is purely imaginary. For ψ_I and ψ_{III} to remain finite as $x \to \pm\infty$, we have to require $A = C' = 0$. From (61) it follows

$$\frac{1+\gamma}{1-\gamma}\, e^{-ik_2a} = \frac{1-\gamma}{1+\gamma}\, e^{ik_2a}. \tag{63}$$

Consider first the case that k_2 is real, i.e. $E^2 \geq (m_0 - V_0)^2$. In consequence γ is purely imaginary by (62) and since the two sides of (63) are then the complex conjugate of each other, we find

$$\mathrm{Im}\left(\frac{1+\gamma}{1-\gamma}\, e^{-ik_2a}\right) = 0. \tag{64}$$

One obtains

$$k_2 \cot k_2 a = \frac{m_0 V_0}{\kappa_1} - \kappa_1, \tag{65}$$

where $\kappa_1 = -ik_1$. This transcendental equation can be solved numerically to yield the energy eigenvalues.

If on the other hand k_2 is purely imaginary, i.e. $E^2 < (m_0 - V_0)^2$, the resulting transcendental equation is

$$(1+\gamma)e^{\kappa_2 a} - (1-\gamma) = 0, \tag{66}$$

where $\kappa_2 = -ik_2$, which again leads to the eigenvalues.

We will now consider the spherically symmetric case in three dimensions, where the potential is given by

$$V(r) = \begin{cases} -V_0 & , r \leq R_0 \\ 0 & , r > R_0 \end{cases}. \tag{67}$$

Consider (7). We now distinguish two cases: First, $k_1^2 = E^2 - (m_0 + V(r))^2 > 0$. Then, by substituting $\varrho = k_1 r$, the first of (7) reads

$$\varrho^2 \frac{\mathrm{d}^2}{\mathrm{d}\varrho^2} g + 2\varrho \frac{\mathrm{d}}{\mathrm{d}\varrho} g + \left(\varrho^2 - \kappa(\kappa+1)\right) g = 0, \tag{68}$$

which leads to the solution

$$g(\varrho) = a_1 j_{l_\kappa}(\varrho) + a_2 y_{l_\kappa}(\varrho), \tag{69}$$

where the j_l and y_l are the regular and irregular spherical Bessel functions [21], respectively, and l_κ is as defined in (8). Using (69), one obtains by virtue of the second of (7) the solutions for the small components

$$f(\varrho) = \frac{\kappa}{\mid \kappa \mid}\,\frac{k_1}{E+m_0+V(r)} \times \left(a_1 j_{l_{-\kappa}}(\varrho) + a_2 y_{l_{-\kappa}}(\varrho)\right). \tag{70}$$

In the second case, $k_2^2 = (m_0 + V(r))^2 - E^2 > 0$. Again, substituting $\tilde{\varrho} = k_2 r$ into (7) leads to

$$\tilde{\varrho}^2 \frac{d^2}{d\tilde{\varrho}^2} g + 2\tilde{\varrho}\frac{d}{d\tilde{\varrho}} g - \left(\tilde{\varrho}^2 + \kappa(\kappa+1)\right) g = 0 \tag{71}$$

with the solution

$$g(\tilde{\varrho}) = \sqrt{\frac{\pi}{2\tilde{\varrho}}}\left(b_1 K_{l_\kappa+1/2}(\tilde{\varrho}) + b_2 I_{l_\kappa+1/2}(\tilde{\varrho})\right). \tag{72}$$

Here, $K_{l_\kappa+1/2}$ and $I_{l_\kappa+1/2}$ are the modified spherical Bessel functions [21]. Again, the solution for f is found to be

$$f(\tilde{\varrho}) = \frac{k_2}{E+m_0+V(r)}\sqrt{\frac{\pi}{2\tilde{\varrho}}} \times \left(-b_1 K_{l_{-\kappa}+1/2}(\tilde{\varrho}) + b_2 I_{l_{-\kappa}+1/2}(\tilde{\varrho})\right). \tag{73}$$

We now investigate the bound state solutions. For $r \leq R_0$ we will first consider $k_1^2 = E^2 - (m_0 - V_0)^2 > 0$, whereas for $r > R_0$ we always have $k_2^2 > 0$, since $V(r) = 0$ and $-m_0 < E < m_0$. Thus for (69) and (70) to be regular at $r = 0$ we have to require $a_2 = 0$, while for $r \to \infty$ (72) and (73) with $b_2 = 0$ hold. As in the one-dimensional case, the energy eigenvalues are obtained by requiring continuity of the wave functions at $r = R_0$, i.e.

$$\frac{g_{\leq}(k_1 R_0)}{f_{\leq}(k_1 R_0)} = \frac{g_{>}(k_2 R_0)}{f_{>}(k_2 R_0)}, \tag{74}$$

where the subscript "$\leq$" refers to the solutions for $r \leq R_0$ and ">" to $r > R_0$. Using (69), (70), (72) and (73) this implies

$$\frac{j_{l_\kappa}(k_1 R_0)}{j_{l_{-\kappa}}(k_1 R_0)} = -\frac{\kappa}{\mid \kappa \mid}\,\frac{k_1}{E+m_0-V_0}\,\frac{E+m_0}{k_2} \times \frac{K_{l_\kappa+1/2}(k_2 R_0)}{K_{l_{-\kappa}+1/2}(k_2 R_0)}. \tag{75}$$

Equation (75) determines the bound state energies if

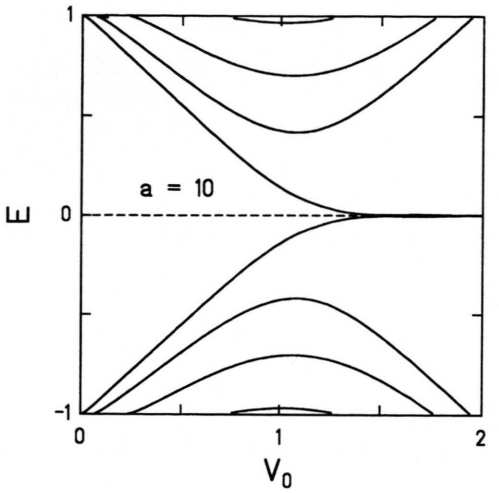

Fig. 8. Energies of bound states in a one-dimensional scalar square-well of depth V_0 and width $a = 10$ Compton wavelenths. The energy of the strongest bound state asymptotically reaches $E = 0$, while the other binding energies vanish as the depth increases.

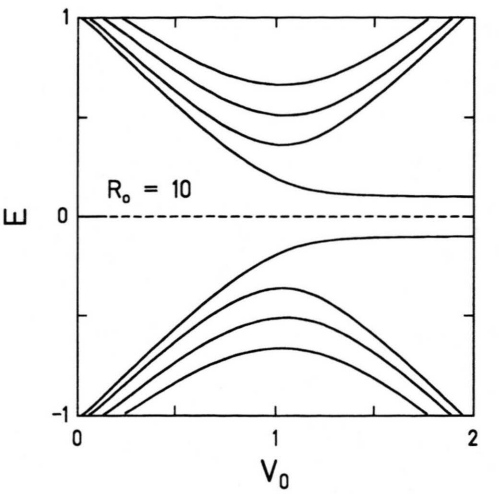

Fig. 9. Energies of bound states in a three-dimensional scalar square-well of depth V_0 and radius $R_0 = 10$ Compton wavelengths. All binding energies except for one state vanish as V_0 increases.

$k_1^2 > 0$ for $r \leq R_0$.

On the other hand, if $\tilde{k}_2{}^2 = (m_0 - V_0)^2 - E^2 > 0$ for $r \leq R_0$, the regularity of (72) and (73) for $r = 0$ requires that $b_1 = 0$. For $r > R_0$, we still have $k_2^2 = m_0^2 - E^2 > 0$ and, replacing k_1 by $\tilde{k}_2$, (74) still holds. We are thus lead to

$$\frac{I_{l_\kappa+1/2}(\tilde{k}_2 R_0)}{I_{l_{-\kappa}+1/2}(\tilde{k}_2 R_0)} = -\frac{\tilde{k}_2}{E + m_0 - V_0} \times \frac{E + m_0}{k_2} \frac{K_{l_\kappa+1/2}(k_2 R_0)}{K_{l_{-\kappa}+1/2}(k_2 R_0)}. \quad (76)$$

Again, the energy eigenvalues are obtained by solving (76) numerically. To determine the remaining free parameters a_1 and b_1, respectively b_1 and b_2, we use the requirement $g_<(k_1 R_0) = g_>(k_2 R_0)$ to obtain

$$\frac{b_1}{a_1} = \sqrt{\frac{2k_2 R_0}{\pi}} \frac{j_{l_\kappa}(k_1 R_0)}{K_{l_\kappa+1/2}(k_2 R_0)}, \quad (77)$$

or $g_<(\tilde{k}_2 R_0) = g_>(k_2 R_0)$, which yields

$$\frac{b_1}{b_2} = \sqrt{\frac{k_2}{\tilde{k}_2}} \frac{I_{l_\kappa+1/2}(\tilde{k}_2 R_0)}{K_{l_\kappa+1/2}(k_2 R_0)}. \quad (78)$$

The last remaining parameter is fixed by the normalization of the wave functions according to (9).

The energy eigenvalues of a fermion in a one-dimensional square well potential are shown in Fig. 8, where the spatial extension of the well was chosen to be 10 Compton wavelengths. Observe that no crossing of the states appears, i.e. no pair creation takes place. All of the bound states except for the strongest bound one disappear as the potential depth increases. The strongest bound state asymptotically reaches $E = 0$ in the one-dimensional case. In this limit any additional vacuum fluctuation may lead to spontaneous pair creation.

Figure 9 displays the energies in the three-dimensional case. The states exhibit essentially the same behavior as in the one-dimensional example. The difference is that the lowest lying state does not approach $E = 0$, but its energy remains finite.

The asymptotical value for $V_0 \to \infty$ is found as follows: First, observe that in the asymptotic region $\tilde{k}_2{}^2 > 0$ holds and that the lowest lying positive energy state corresponds to $\kappa = -1$. Using (8) and (76) we thus have to evaluate $E(R_0)$ for $V_0 \to \infty$ from

$$\frac{1}{E + m_0 - V_0} - \frac{\tilde{k}_2 R_0}{E + m_0 - V_0} \coth\left(\tilde{k}_2 R_0\right) = \frac{1}{E + m_0} + \frac{k_2 R_0}{E + m_0}. \quad (79)$$

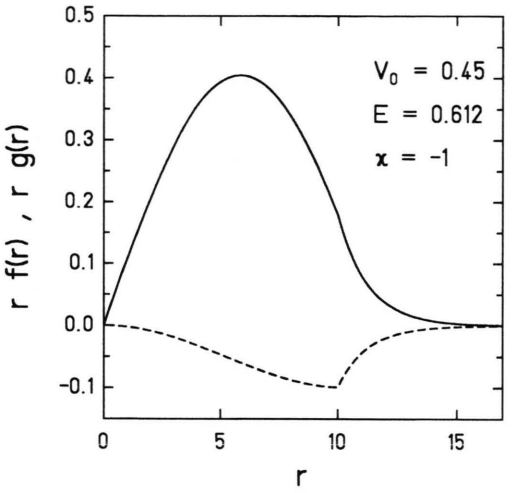

Fig. 10. Bound state wave function in a three-dimensional scalar square-well with $R_0 = 10$. $\kappa = -1$ corresponds to a s-state. The solid line depicts $rg(r)$ while the dashed line displays $rf(r)$.

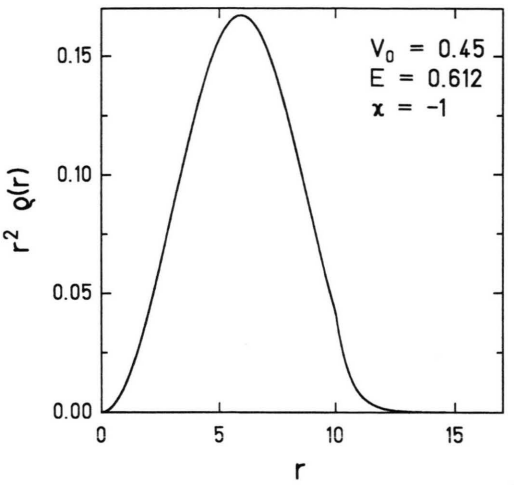

Fig. 11. Probability density ϱr^2 of the state depicted in Figure 10.

The first term vanishes for $V_0 \to \infty$ while the second term approaches R_0 in this limit. We thus find for $V_0 \to \infty$

$$R_0 = \frac{1}{m_0 + E} + \frac{k_2 R_0}{E + m_0}. \tag{80}$$

Solving this equation for E one finally arrives at

$$E(R_0) \overset{V_0 \to \infty}{=} -\frac{1}{2} m_0 + \frac{1}{2R_0} + \frac{\sqrt{m_0^2 R_0^2 + 2 m_0 R_0 - 1}}{2R_0}. \tag{81}$$

Considering continuum states, we have $\mid E \mid > m_0$ and we assume $k_1^2 > 0$ for all r. The continuity conditions then read, using $\tilde{k}_1 = \sqrt{E^2 - m_0^2}$,

$$\begin{aligned} g_{<}(k_1 R_0) &= g_{>}(\tilde{k}_1 R_0), \\ f_{<}(k_1 R_0) &= f_{>}(\tilde{k}_1 R_0). \end{aligned} \tag{82}$$

Since the y_l remain finite as $r \to \infty$, (69) and (70) yield

$$a_1 j_{l_\kappa}(k_1 R_0) = b_1 j_{l_\kappa}(\tilde{k}_1 R_0) + b_2 y_{l_\kappa}(\tilde{k}_1 R_0) \tag{83}$$

and

$$\frac{k_1}{E + m_0 - V_0} a_1 j_{l-\kappa}(k_1 R_0) = \frac{\tilde{k}_1}{E + m_0} \left(b_1 j_{l-\kappa}(\tilde{k}_1 R_0) + b_2 y_{l-\kappa}(\tilde{k}_1 R_0) \right). \tag{84}$$

Equations (83) and (84) determine the coefficients b_1 and b_2 for a given energy and V_0 as functions of a_1, which is fixed by normalization. Employing the asymptotical behaviour of the exterior solution,

$$\begin{aligned} g(r) &\overset{r \to \infty}{\to} A \frac{\sin(\tilde{k}_1 r + \delta)}{r}, \\ f(r) &\overset{r \to \infty}{\to} A \frac{\tilde{k}_1}{E + m_0} \frac{\cos(\tilde{k}_1 r + \delta)}{r}, \end{aligned} \tag{85}$$

with some normalization factor A one can also evaluate the scattering phase δ.

Some examples of bound state wave functions are displayed in Figs. 10 to 13. Figure 10 depicts the strongest bound state, corresponding to the 1s-state, at a potential depth of $V_0 = 0.45\, m_0$. The wave functions as well as the probability density shown in Fig. 11 are continuous but not differentiable at $r = R_0$ due to the discontinuity in the potential. In Figs. 12 and 13 the same state is displayed, the potential depth now being $V_0 = 1.5\, m_0$. In this region, the higher states are increasingly less bound.

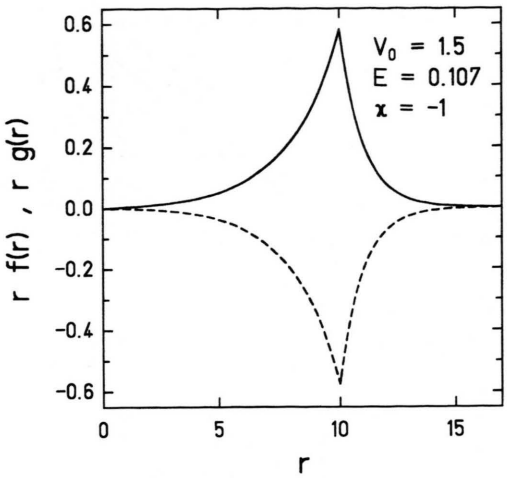

Fig. 12. Same as Fig. 10, but with $V_0 = 1.5$, where $E = 0.107$ in natural units with $m_0 = 1$.

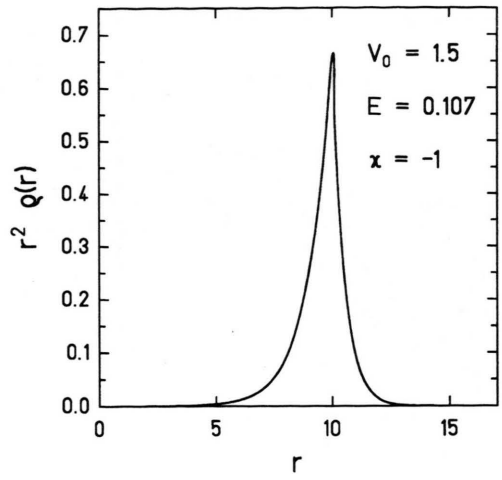

Fig. 13. Probability density ϱr^2 of the state displayed in Fig. 12 ($E = 0.107, \kappa = -1$).

6. Linear and quadratic potentials

Scalar potentials of the form

$$V(r) = \frac{\lambda}{r} + \eta^2 r + \omega^3 r^2 \tag{86}$$

are of interest because they exhibit confinement properties. The Dirac equation for the linear potential was solved by Critchfield [5], the quadratic potential has been discussed by various authors [6] - [8]. In general, Su and Ma have schown that confinement is possible only if the scalar potential is stronger than the potential coupled as the time-like component of a four-vector to the same power of r [9]. We will compute a series solution for the general type of potential given in (86). Energy eigenvalues are compared with those obtained by Critchfield [5] and Ram and Arafah [8] for special cases. It is verified that confinement exists in either case.

The radial equations read

$$\begin{aligned} 0 &= \frac{\mathrm{d}}{\mathrm{d}r}g + \frac{\kappa+1}{r}g \\ &\quad - \left(E + m_0 + \frac{\lambda}{r} + \eta^2 r + \omega^3 r^2\right) f, \\ 0 &= \frac{\mathrm{d}}{\mathrm{d}r}f - \frac{\kappa-1}{r}f \\ &\quad + \left(E - m_0 - \frac{\lambda}{r} - \eta^2 r - \omega^3 r^2\right) g. \end{aligned} \tag{87}$$

Please note that our definition of κ differs from that used by Critchfield and Ram et al. From the ansatz

$$\begin{aligned} g(r) &= \phi(r)\, r^{\gamma-1} \\ &\quad \times \exp(-m_0 r - \frac{1}{2}\eta^2 r^2 - \frac{1}{3}\omega^3 r^3), \\ f(r) &= \varphi(r)\, r^{\gamma-1} \\ &\quad \times \exp(-m_0 r - \frac{1}{2}\eta^2 r^2 - \frac{1}{3}\omega^3 r^3), \end{aligned} \tag{88}$$

the following differential equations for the functions $\phi(r)$ and $\varphi(r)$ are derived

$$\begin{aligned} 0 &= \frac{\mathrm{d}}{\mathrm{d}r}\phi + \frac{\gamma+\kappa}{r}\phi - \left(m_0 + \eta^2 r + \omega^3 r^2\right)\phi \\ &\quad - \left(E + m_0 + \frac{\lambda}{r} + \eta^2 r + \omega^3 r^2\right)\varphi, \\ 0 &= \frac{\mathrm{d}}{\mathrm{d}r}\varphi + \frac{\gamma-\kappa}{r}\varphi - \left(m_0 + \eta^2 r + \omega^3 r^2\right)\varphi \\ &\quad + \left(E - m_0 - \frac{\lambda}{r} - \eta^2 r - \omega^3 r^2\right)\phi. \end{aligned} \tag{89}$$

By examining (89) for small values of r one has $\gamma = \sqrt{\kappa^2 + \lambda^2}$. Substituting $P(r) = \phi(r) + \varphi(r)$

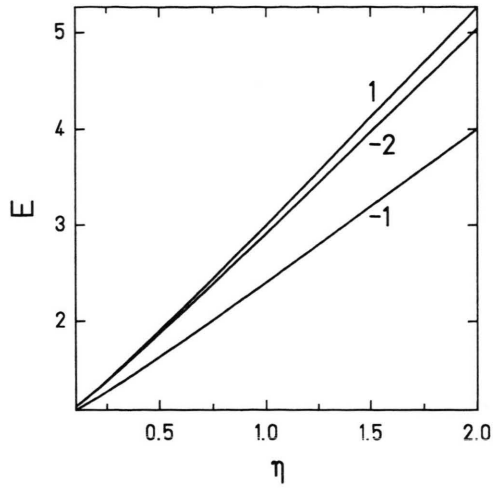

Fig. 14. Energy eigenvalue E of a Dirac particle with m_0 = 1 in a scalar linear potential versus the coupling strength parameter η. The lowest states with κ = -1, -2 and 1 are considered; $\lambda = 0$.

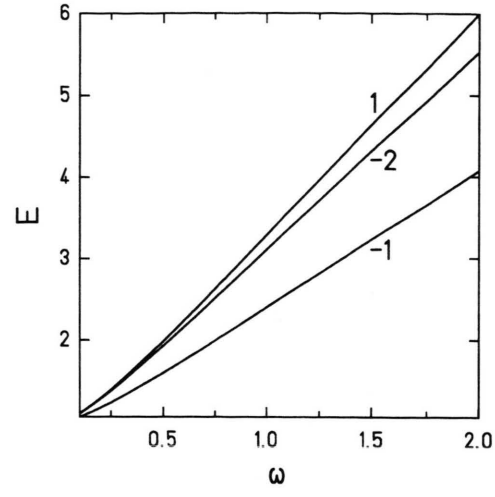

Fig. 15. Energy eigenvalue E of a Dirac particle with m_0 = 1 in a scalar quadratic potential versus the coupling strength parameter ω. The lowest states with κ = -1, -2 and 1 are considered; $\lambda = 0$.

and $Q(r) = \phi(r) - \varphi(r)$ one readily arrives at

$$0 = \frac{\mathrm{d}}{\mathrm{d}r}P + \left\{\frac{\gamma-\lambda}{r} - 2m_0 - 2\left(\eta^2 r + \omega^3 r^2\right)\right\} P + \left(E + \frac{\kappa}{r}\right) Q,$$

$$0 = \frac{\mathrm{d}}{\mathrm{d}r}Q + \frac{\gamma+\lambda}{r}Q - \left(E - \frac{\kappa}{r}\right) P. \qquad (90)$$

Assuming P and Q to be power series,

$$P(r) = \sum_{k=0}^{\infty} p_k\, r^k,\ Q(r) = \sum_{k=0}^{\infty} q_k\, r^k, \qquad (91)$$

the following relations must hold:

$$0 = -2\omega^3 p_{k-2} - 2\eta^2 p_{k-1} - 2m_0 p_k + (k+1+\gamma-\lambda)p_{k+1} + E q_k + \kappa q_{k+1},$$

$$0 = -E p_k + \kappa p_{k+1} + (k+1+\gamma+\lambda)q_{k+1}. \qquad (92)$$

Using the second of (92) to express q_k and q_{k+1} in terms of the p_i, one finally has

$$A_k p_{k+1} + B_k p_k + C_k p_{k-1} + D_k p_{k-2} = 0 \qquad (93)$$

where

$$A_k = \kappa^2(k+\gamma+\lambda) - (k+1+\gamma+\lambda) \times (k+\gamma+\lambda)(k+1+\gamma-\lambda),$$

$$B_k = 2m_0(k+1+\gamma+\lambda)(k+\gamma+\lambda) + E\kappa,$$

$$C_k = 2\eta^2(k+1+\gamma+\lambda)(k+\gamma+\lambda) - E^2(k+1+\gamma+\lambda),$$

$$D_k = 2\omega^3(k+1+\gamma+\lambda)(k+\gamma+\lambda). \qquad (94)$$

Since p_k vanishes for $k < 0$, from (93) it follows $A_0 p_1 + B_0 p_0 = 0$, where p_0 is a normalization factor. Assuming $\omega \neq 0$, (93) and (94) lead to

$$k p_{k+1} \to 2m_0 p_k + 2\eta^2 p_{k-1} + 2\omega^3 p_{k-2} \qquad (95)$$

as $k \to \infty$. Then the normalizability of the wave function requires that [5] $b_{k+1} = b_k\{1 + O(1/k)\} < 0$, where $b_k = p_k/p_{k-1}$. Defining further $H_k = A_k/B_k$, $M_k = C_k/B_k$, $L_k = D_k/B_k$, (93) can be rewritten as

$$b_{k-1} = -\frac{L_k}{b_k + M_k + H_k b_k b_{k+1}}. \qquad (96)$$

A procedure to determine the eigenvalues is described in [5].

However, for our numerical determination of the

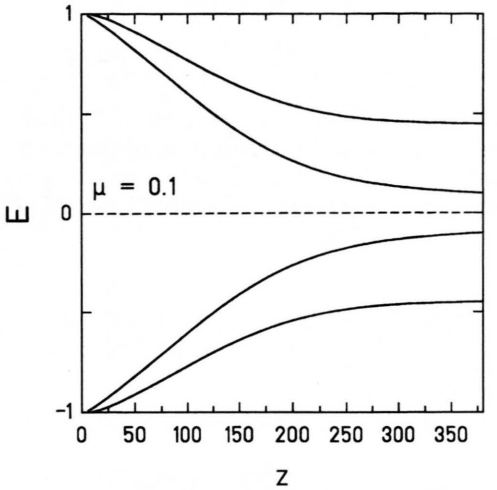

Fig. 16. Energy eigenvalue E of the strongest bound states for the scalar exponential potential versus the coupling strength parameter Z. For positive energies s-states are considered. The range parameter of the exponential potential is fixed to $\mu = 0.1$.

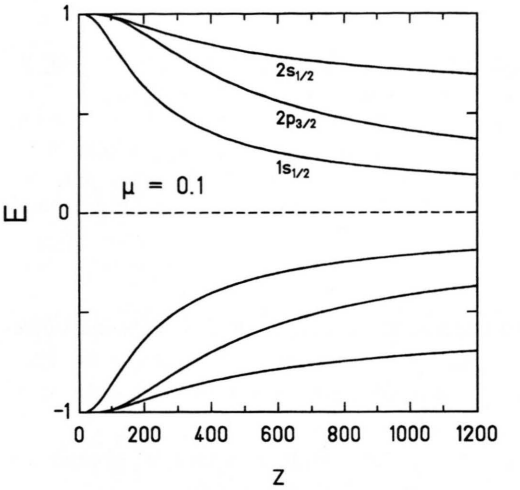

Fig. 17. The same as in Fig. 16 for a scalar Yukawa potential.

energy eigenvalue we found it more convenient to employ similar procedures as in [22]. For the special case $m_0 = 0$ and for a scalar linear potential we obtained perfect agreement with the tabulated data of Critchfield [5], while for scalar linear and quadratic potentials we achieved fair agreement with the approximative results of Ram and Arafah [8].

For a limited parameter range for η and $m_0 = 1$ the energy eigenvalues E of the lowest states with κ = -1, -2 and 1 are displayed in Fig. 14 for a scalar linear potential ($\omega = 0$). For large η we obviously find an almost linear dependence which allows for simple extrapolations. Equivalently, we show in Fig. 15 the computed energy eigenvalues for a scalar quadratic potential ($\eta = 0$) as function of the coupling strength ω. The functional dependene $E(\omega)$ is very similar to the case discussed before.

7. Yukawa and exponential potential

As additional examples for scalar short-range interactions we evaluate solutions of the radial Dirac equation for a Yukawa potential

$$V(r) = -\frac{Z\alpha}{r} \exp(-\mu r) \tag{97}$$

as well as for an exponential potential

$$V(r) = -Z\alpha \exp(-\mu r) \tag{98}$$

with the range parameter μ. Again, the coupling strength is determined by $Z\alpha$. For the potentials (97) and (98) we solved the radial equations numerically employing the techniques as described in [23].

The exponential potential (98) is finite at the origin and thus does not differ considerably from the three-dimensional square-well potential. The numerical integration is started for $r \to 0$ üsing the initial values (69) and (70) with $a_2 = 0$ and the potential (98). In contrast to this the Yukawa potential (97) exhibits an $1/r$-behavior close to the origin. Consequently, we start the numerical integration for $r \to 0$ with the initial values (12) and (17).

The energy eigenvalues for the most strongly bound states in the exponential potential (98) with $\mu = 0.1$ are displayed in Fig. 16 as function of the coupling strength parameter Z. For positive energies s-states are considered. Beyond $Z \simeq 200$ there are only slight modifications of the energy eigenvalues. The dependence of E on the potential depth displays some similarity with the results for a Coulomb-like potential (Fig. 1) and for the three dimensional square-well potential (Figure 9).

Correspondingly, the energy eigenvalues for some innermost bound states in the singular Yukawa potential (97) with $\mu = 0.1$ are plotted in Figure 17. Again compared with the outcome for a pure $1/r$ - potential (cf. Fig. 1) the dependence of E on Z for a scalar Yukawa potential is not drastically modified.

8. Conclusions

We have solved the Dirac equation for various types of scalar potentials which are coupled to the mass. In our investigations special emphasis was laid on the strong coupling limit for the scalar interaction for which there is no spontaneous pair creation. We explicitly derived eigenvalues and normalized wave functions for bound states as well as for continuum states.

Acknowledgement

One of us (B.B.) would like to thank GSI for the kind hospitality during the preparation of this work. We also thank Axel Saalfeld for interesting discussions. We acknowledge support by BMFT and DFG.

[1] W. Greiner, B. Müller and J. Rafelski, Quantum Electrodynamics of Strong Fields, Springer, Berlin, 1985.

[2] M. K. Sundaresan and P. J. S. Watson, Phys. Rev. Lett. **29**, 15 and 1122 (1972).

[3] A. Schäfer, J. Reinhardt, B. Müller, W. Greiner, and G. Soff, J. Phys. G **11**, L69 (1985).

[4] J. Vasconcelos, Rev. Bras. Fis. **1**, 441 (1971).

[5] Ch. L. Critchfield, J. Math. Phys. **17**, 261 (1976).

[6] B. Ram and R. Halasa, Lett. Nuovo Cim. **26**, 551 (1979).

[7] B. Ram, Lett. Nuovo Cim. **28**, 476 (1980).

[8] B. Ram and M. Arafah, Lett. Nuovo Cim. **30**, 5 (1981).

[9] R.-K. Su and Z.-Q. Ma, J. Phys A **19**, 1739 (1986).

[10] H. W. Crater and P. V. Alstine, Phys. Rev. D **36**, 3007 (1987).

[11] G. Soff, B. Müller, J. Rafelski, and W. Greiner, Z. Naturforsch. **28a**, 1389 (1973).

[12] H. G. Dosch, J. H. D. Jensen, and V. F. Müller, Physical Norwegica **5**, 2 (1971).

[13] P. J. Mohr, in: Physics of Strong Fields, ed.: W. Greiner, p. 17, NATO ASI series Vol. **153**, Plenum, New York 1986.

[14] V. P. Iyer and L. K. Sharma, Phys. Lett. **102B**, 154 (1981).

[15] F. Ravndal, Phys. Lett. **113B**, 57 (1982).

[16] G. V. Shishkin, J. Phys. **A26**, 4135 (1993).

[17] S. Ikhdair, O. Mustafa, and R. Sever, Hadronic Journ. **16**, 57 (1993).

[18] M. E. Grypeos, C. G. Koutroulos, and G. J. Papadopoulos, Phys. Rev. **A50**, 29 (1994).

[19] M. E. Rose, Relativistic Electron Theory, John Wiley, New York, 1961.

[20] K. Bechert, Ann. Phys. **6**, 700 (1930).

[21] M. Abramowitz and I. A. Stegun, Handbook of Mathematical Functions, Dover Publications, New York 1965.

[22] W. Fleischer and G. Soff, Z. Naturforsch. **39a**, 703 (1984).

[23] H.-J. Bär and G. Soff, Physica **128C**, 225 (1985).